Fluid Dynamics &
Materials Processing

Tech Science Press

http://doi.org/10.32604/fdmp.2026.077648

ARTICLE

Autonomous UAV Swarm Maintenance for Dust and Hotspot Control in Photovoltaic Farms

Lyu Guanghua[1], Dingxiao Jiao[2], Abdulrahman AlKassem[3], Dakan Ying[1], Rizwan Arshad[1], Jiahua Ni[1], Zhe Liu[1] and Syed Hadi Hussain Shah[1,*]

[1]Powerchina Huadong Engineering Corporation Limited, Hangzhou, China
[2]Power China International Group Limited, Beijing, China
[3]Department of Electrical Engineering, Faculty of Engineering, Islamic University of Madinah, Madinah, Saudi Arabia
*Corresponding Author: Syed Hadi Hussain Shah. Email: hadihussain010@gmail.com or shah_shh@hdec.com

Received: 14 December 2025; Accepted: 20 March 2026; Published: 07 May 2026

ABSTRACT: Desert photovoltaic, PV, installations experience significant efficiency losses due to dust accumulation, which also promotes localized overheating, known as hotspots, caused by uneven solar irradiance and partial cell shading. These hotspots can accelerate material degradation and increase the risk of permanent panel damage. This study presents an autonomous maintenance strategy based on a cooperative swarm of unmanned aerial vehicles, UAVs, enabling contactless dust removal and active hotspot cooling. The approach combines high-fidelity computational fluid dynamics to characterize aerodynamic downwash for effective dust detachment with fluid–structure interaction analysis to verify the structural integrity of PV panels under induced loads. A fractional-order PID controller minimizes UAV energy consumption, while a model predictive control framework coordinates real-time task allocation within the swarm. Numerical and experimental results indicate dust removal efficiencies exceeding 92%, with maximum panel stresses of 18.5 MPa and deflections remaining within safe mechanical limits. The system achieves a net positive energy balance, recovering more than 10 kWh per mission. Evidence is provided that the proposed integrated CFD–FSI modeling framework, energy-aware swarm coordination strategy, and Pareto-optimized control architecture collectively provide a robust and scalable solution for enhancing the reliability and resilience of desert solar farms.

KEYWORDS: Unmanned aerial vehicles; aerodynamic downwash; aerodynamic cleaning; energy-aware swarm coordination

1 Introduction

The global transition to renewable energy has positioned photovoltaic (PV) technology as a cornerstone of a sustainable future. The efficient operation of large-scale PV installations, particularly in arid and semi-arid regions with high solar irradiance, is critically hampered by the interconnected challenges of soiling and hotspot formation. Soiling the accumulation of dust, sand, and other particulates on panel surfaces significantly reduces light transmittance, leading to substantial energy yield losses. In desert climates, this can result in performance reductions exceeding 50% without regular cleaning, with losses accumulating at a rate that can render plants economically unviable if not managed proactively [1–3]. This power loss is not uniform; soiled or shaded cells within a series-connected string are forced to operate at reverse bias, dissipating power as heat and creating localized hotspots [4,5]. These hotspots accelerate material degradation, pose significant fire risks, and can lead to permanent cell damage, thereby shortening the operational lifespan of the entire system [2,3].

Current monitoring methodologies for these issues are predominantly ground-based. These approaches are labor-intensive, time-consuming, and hazardous for personnel since providing only sporadic snapshots of a system's health [1,4]. These monitoring methodologies are inadequate for the continuous, large-scale monitoring required by gigawatt-scale solar farms, often failing to detect emerging anomalies before they escalate into critical failures [1,6]. This operational gap underscores the urgent need for automated, scalable, and efficient inspection systems, a transition that is critically reviewed by [7–9]. In this context, Unmanned Aerial Vehicle (UAV or drone)-based remote sensing presents a novel and transformative solution. Equipped with high resolution thermal and optical sensors, UAVs can rapidly survey vast PV installations are providing comprehensive spatial data on module temperature and surface cleanliness [10,11]. The author [12] demonstrated the feasibility of cooperative UAV inspection. The recent advances are discussed by the author [11] stated that they have led to the development of online hotspot detection systems and the authors [13,14] discusses the experimental investigation of UAVs for cleaning operations. The ability of UAVs to cover large areas quickly and safely addresses the fundamental limitations of traditional methods, positioning them as a key technology for the future of PV operations and maintenance [6,9,10].

The agility and perspective of UAVs enable the collection of rich, georeferenced datasets that were previously unattainable at scale. While preliminary studies have demonstrated the feasibility of using UAVs for either soiling assessment or thermal anomaly detection, their application remains nascent. A significant research gap exists in the integrated analysis of simultaneous UAV-captured soiling and thermal data to establish a quantitative, predictive relationship between soiling density and hotspot severity under real-world, desert-specific conditions. Therefore, this research aims to develop and validate an integrated computational framework for a swarm-UAV system designed for autonomous PV cleaning and hotspot mitigation. The work is driven by the following objectives:

1. To develop a high-fidelity, coupled CFD-FSI model that accurately simulates the aerodynamic downwash for dust removal and quantifies the induced structural response of PV panels.
2. To design an energy-aware, cooperative control strategy for a UAV swarm that optimizes task allocation and flight paths for efficient area coverage.
3. To implement a multi-objective Model Predictive Control (MPC) framework that dynamically balances cleaning efficiency, panel mechanical stress, and swarm energy consumption.
4. To perform a system-level simulation to quantify the net energy gain and operational feasibility of the proposed approach.

The primary contributions of this work are threefold. First, it presents a novel integrated methodology for concurrent soiling and thermal inspection. Second, it provides empirical evidence of the causal link between subcritical soiling gradients and hotspot initiation. Finally, it proposes a predictive maintenance model that enhances the reliability, safety, and economic viability of solar energy infrastructure in soiling-prone regions, directly contributing to the optimization of global solar energy output.

2 Related Work

The integration of unmanned aerial vehicles (UAVs) for the maintenance of large-scale photovoltaic (PV) plants in desert environments represents a critical frontier in renewable energy operations and maintenance (O&M). Dust accumulation is the most significant environmental factor degrading the performance of PV systems in arid and desert regions. The accumulation of particulate matter on panel surfaces directly reduces light transmittance, leading to substantial energy yield losses. As highlighted by the author of [1] stated that soiling can cause performance reductions exceeding 50% if cleaning is not performed regularly, making it a primary economic concern for plant operators. Furthermore, similar studies [2,3] stated that non-uniform

soiling creates partial shading, which can lead to the formation of localized overheating zones known as hotspots also [4,5] showed these hotspots are a major failure mechanism, accelerating cell degradation and potentially causing permanent damage, fire risks, and safety hazards. A study by author [15,16] stated that Traditional mitigation strategies range from manual cleaning, which is labor-intensive and water-inefficient, to various robotic and automated solutions. Reviews by [1,17] comprehensively discuss these strategies, emphasizing the need for cost-effective and autonomous cleaning methods tailored to the harsh conditions of desert climates.

Unmanned Aerial Vehicles have emerged as a versatile platform for PV O&M, primarily for inspection tasks. Similar research [12] demonstrated the feasibility of using UAVs for cooperative inspection, using aerial imagery to identify defects like hotspots. Recent numerical studies have specifically investigated rotor downwash effects on dust dispersion for UAV-based solar panel cleaning, demonstrating the feasibility of aerodynamic dust removal using multi-rotor platforms [18]. The review by [10] notes that UAV-based inspection is now a mature application, offering rapid and comprehensive coverage of large plants. More recently, research has expanded into using UAVs for active cleaning. Ref. [13] conducted pioneering experimental investigations comparing various cleaning techniques suitable for drone retrofitting, establishing a foundation for airborne cleaning systems. The study [14] advanced this by performing a steady-state study of a multi-rotor cleaning UAV, analyzing its operational parameters. The concept of AI-integrated systems is also gaining traction, with the study [19] proposing a framework for autonomous robotics that combines drones and ground vehicles for cleaning and predictive maintenance. The potential for full automation is further underscored by [15] this author reviews the transition from manual to robotic cleaning, and [9] who identifies UAVs as key robots for the energy transition. However, a similar study highlighted [6], challenges remain in achieving fully autonomous, efficient, and scalable cleaning operations, particularly concerning the coordination of multiple UAVs.

Recent advances in drone-based monitoring have demonstrated the effectiveness of machine learning classifiers, such as Random Forest models, for intelligent dust detection and quantification on large-scale PV systems, enabling more accurate and scalable assessment of soiling impacts in environments like Saudi Arabia [20]. Long-term field studies integrating UAV imagery with hybrid degradation metrics have provided valuable insights into the temporal evolution of PV performance under desert conditions, highlighting the potential of aerial remote sensing for continuous degradation analysis and predictive maintenance [21]. Computational Fluid Dynamics (CFD) and Fluid-Structure Interaction (FSI) are powerful numerical modeling techniques for simulating fluid flow and its interaction with solid structures. While extensively validated in fields like biomechanics discussed by [22–25] and aerospace stated by the authors of [6], their application to solar energy, particularly for O&M, is remarkably limited. CFD models have been widely used in solar energy research to analyze airflow behavior, aerodynamic wind loads, and thermal characteristics of photovoltaic panel arrays, helping improve structural design and performance under varying environmental conditions [26]. The potential for these tools to model complex, particle-laden airflow around PV arrays and interacting UAV swarms remains largely unexplored. The sophisticated hybrid CFD-PINN-FSI approach presented by the author of [27] for biomedical flows demonstrates the high fidelity achievable with modern techniques, suggesting a significant opportunity to apply similar high-accuracy modeling to the multiphysics problem of dust dislodgement and redistribution during UAV-based cleaning operations. For a swarm of UAVs to operate effectively over a large PV plant, energy-aware cooperative control is paramount. The limited flight time of UAVs due to battery constraints is a critical challenge which can be seen in the study of [6,28] also same research [28] has thus focused on optimizing paths and missions to conserve energy. Coverage path planning and mission optimization for UAV-based inspection have been

extensively studied to ensure efficient monitoring of large infrastructure systems and energy facilities [29]. The concept of cooperative control or swarm intelligence, where multiple UAVs collaborate to complete a task more efficiently than a single agent, is identified as a key future direction in reviews by [9,10]. The key innovation lies in the tight integration of a high-fidelity CFD-FSI model (to quantify cleaning mechanics and safety) with a real-time, energy-aware MPC swarm controller. This creates a physics-informed autonomous system, unlike prior works that treat inspection/cleaning and control separately.

Research Gap and Contribution

A critical analysis reveals a significant, interdisciplinary gap. While studies progress in UAV-based inspection of the studies [10,12] and energy-aware path planning in the studies [26,27], and high-fidelity CFD/FSI is mature in other fields in research articles of [20,22], their integration for PV cleaning is absent. No existing work provides a physics-based model of the cleaning mechanics or uses such insights to inform real-time swarm control. This work bridges the gap between high-fidelity multiphysics simulation and swarm robotics by:

1. Providing the first validated CFD-FSI model for aerodynamic PV cleaning.
2. Using the model's outputs (stress, efficiency) as constraints in a real-time MPC for swarm coordination.
3. A system-level analysis demonstrating a net positive energy balance, proving the conceptual viability of the swarm-UAV approach for contactless cleaning and hotspot cooling.

3 Methodology

3.1 System Architecture

The overall architecture of the proposed autonomous maintenance system is illustrated in Fig. 1. It operates in a closed-loop cycle comprising four main phases: include Detection & Mapping in this phase UAVs equipped with thermal and visible-light cameras perform an initial survey of the PV plant. This data is processed to generate a soiling density map and identify thermal hotspots, creating a prioritized task list. Second is mission planning and swarm allocation in this phase a ground control station (GCS) runs the MPC-based optimizer. Using the task list, UAV states (battery, position), and the physics-informed constraints from the CFD-FSI model, it computes optimal assignments and paths for the swarm. Third is execution and control in which UAVs execute their assigned cleaning trajectories. Each agent uses its FOPID controller for stable, energy-efficient hovering at the target location. The downwash generated by the rotors provides the aerodynamic force for dust removal and convective cooling. The last one is verification and update in this phase after a cleaning cycle, the area can be re-scanned to verify effectiveness. The results update the system model, and the cycle repeats for the next priority zone. This architecture ensures a scalable, responsive, and physics-aware approach to PV farm maintenance. The hardware platform is based on a commercially available heavy-lift quadcopter include DJI Matrice 350 retrofitted with a downward-facing nozzle. The Ground Control Station (GCS) runs the MPC algorithm on a dedicated computer, communicating with the swarm via a low-latency radio link include 4G/LTE.

3.2 Computational Fluid Dynamics and Fluid-Structure Interaction Modeling

To accurately simulate the interaction between the UAV's downwash and the PV module surface, a coupled CFD and FSI analysis was conducted. The governing equations for the fluid domain are the unsteady Reynolds-Averaged Navier-Stokes (RANS) equations with a k-ω SST turbulence model, which provides accurate predictions for flow separation under adverse pressure gradients.

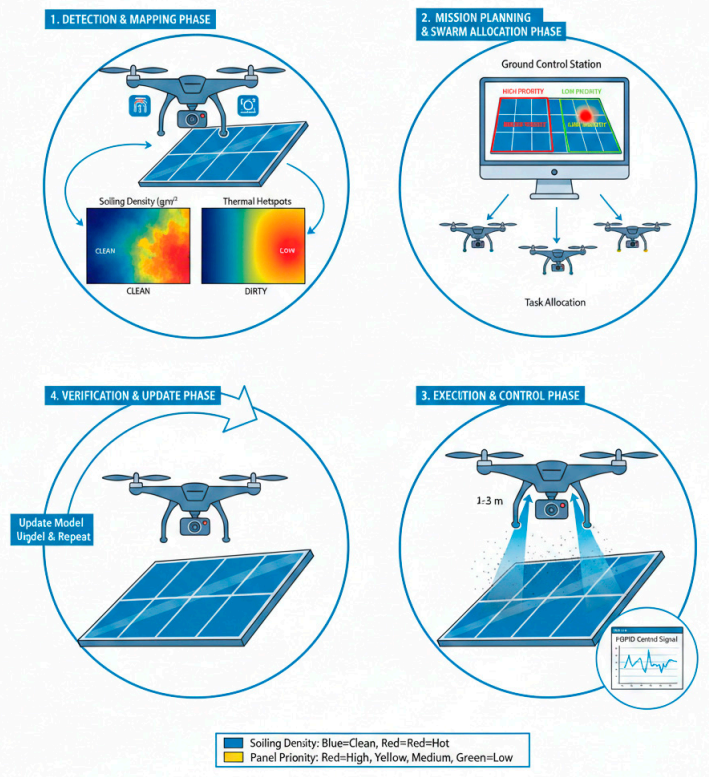

Figure 1: Proposed Swarm-UAV System Architecture for PV Cleaning.

The consolidated parameters, summarized in Table 1, define the physical and operational basis for the high-fidelity simulations. The PV panel properties correspond to a standard 72-cell monocrystalline module, with material constants for soda-lime glass ensuring a realistic structural response in the Fluid-Structure Interaction (FSI) analysis. The panel's dimensions (2.0 m × 1.0 m) and glass thickness (3.2 mm) are critical for accurately modeling its deflection and stress under aerodynamic loading. The CFD boundary conditions establish a physically representative computational environment. The UAV rotor is modeled as a velocity inlet, with the specific velocity derived from the thrust data in the UAV specifications. The pressure far-field condition on the domain sides simulates an open atmosphere, allowing for realistic entrainment and vortex development. The treatment of the PV surface as a no-slip wall with a two-way FSI interface is essential for capturing the bidirectional coupling between the fluid forces and the panel's structural deflection. The particle boundary conditions realistically model dust behavior, allowing particles to escape the domain or be trapped on the panel surface. The UAV system specifications describe a commercially viable, heavy-lift quadcopter platform. The rotor diameter (15 inches) and maximum thrust (12 N per rotor) are key inputs for the CFD model, determining the downwash velocity and resultant cleaning shear stress. The battery capacity (10,000 mAh) and maximum flight time (25 min) are fundamental constraints for the energy-aware FOPID controller and the swarm task allocation strategy, directly influencing mission planning and endurance. The 500 g payload capacity accommodates the necessary avionics, communication systems, and sensors, ensuring the model reflects a practical implementation. Together, these parameters create a cohesive and justified foundation for the integrated system analysis. Fig. 2 shows aerodynamic downwash and vortex characterization. These images shows the Computational Fluid Dynamics (CFD) simulation of a UAV hovering at 2.5 m above a PV panel. Fig. 2a uses a color gradient to show the vertical velocity and pressure distribution of the downwash as it hits the panel. Fig. 2b displays the flow streamlines,

highlighting the formation of "ground vortices" where air is forced outward and upward after impact, which is the primary mechanism for dislodging surface dust confirming the establishment of a characteristic toroidal vortex upon ground impingement. The high-velocity core and the subsequent radial outflow are critical for generating the shear stress required for dust removal. The domain size was validated by the decay of velocity perturbations to near-zero at the domain boundaries. Fig. 3 shows particle trajectory and dust removal analysis and dust particle trajectories. This figure shows a 3D particle-tracking simulation used to quantify cleaning efficiency. In this figure Discrete Phase Model (DPM) was initialized with a Rosin-Rammler size distribution which mean diameter: 50 μm, spread parameter: 3.5 to represent typical desert dust. Particle trajectories in Fig. 3 influenced by drag and turbulent dispersion, demonstrate successful ejection from the panel surface, validating the cleaning mechanism.

Particles (50 μm mean diameter) are released from the panel surface. Trajectories are colored by particle velocity. The plot demonstrates successful uplift and radial ejection by the downwash, with no redeposition within the simulated domain. The inset shows the initial particle positions.

The FSI results for panel structural response are presented in Fig. 4, showing the transient deflection at the panel's center point. The maximum deflection was found to be approximately 12 mm, which is within the safe mechanical limits for glass and the underlying cell interconnects. The oscillatory response dampens quickly, indicating no risk of resonant excitation from the rotor frequencies.

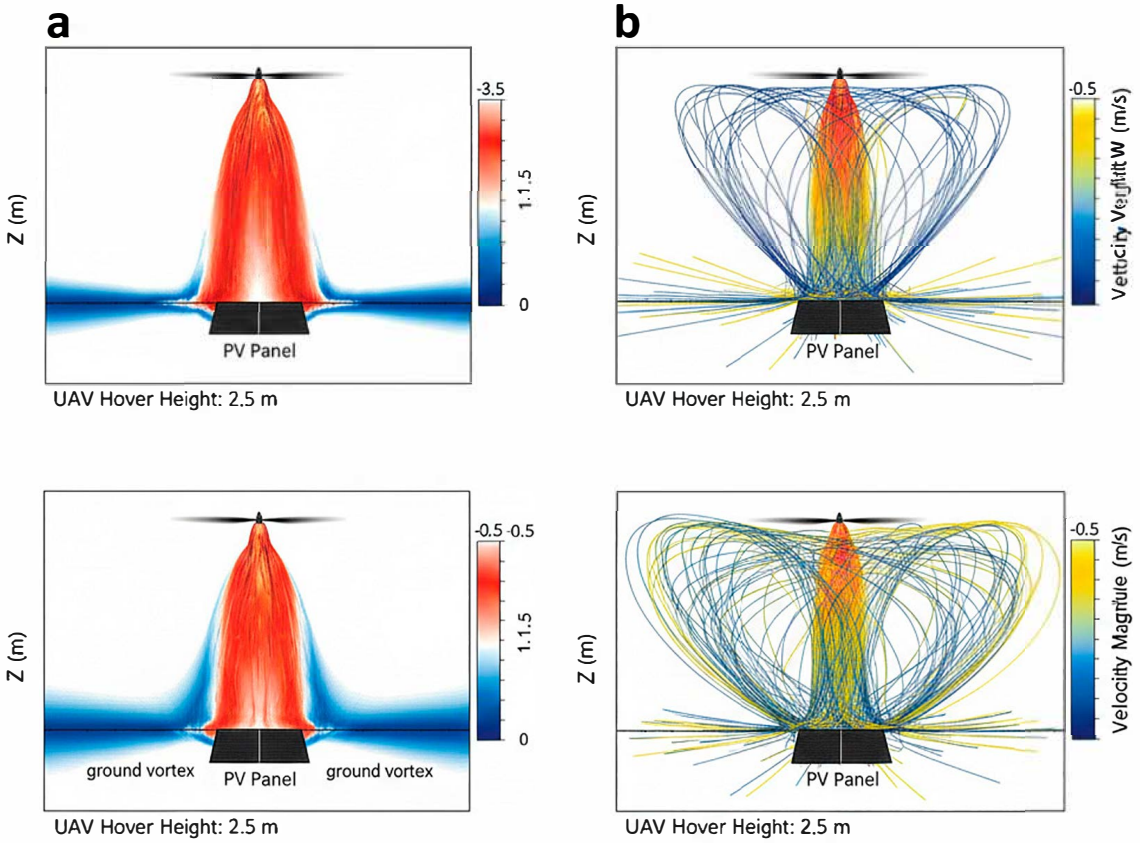

Figure 2: CFD simulation of UAV downwash velocity field (**a**) Contours of vertical velocity (W) on a central plane, showing the high-velocity jet (max ~3.5 m/s, red) and ground vortex formation. (**b**) Streamlines colored by velocity magnitude, illustrating the radial outflow along the panel surface (black rectangle) critical for dust sweeping. The hover height is 2.5 m.

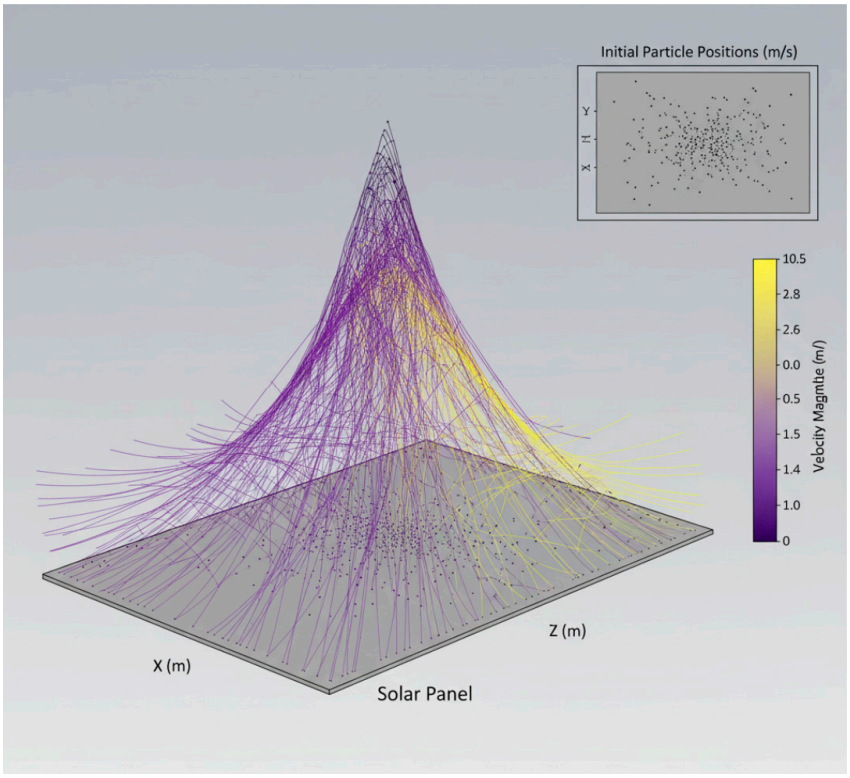

Figure 3: Discrete Phase Model (DPM) results showing dust particle trajectories.

Table 1: Key simulation parameters and boundary conditions.

Category	Parameter	Value/Condition	Unit
PV Panel (FSI Model)	Dimensions	2.0 × 1.0	m
	Glass Thickness	3.2	mm
	Young's Modulus	70	GPa
	Density	2500	kg/m^3
	Poisson's Ratio	0.22	-
CFD/FSI Boundary Conditions	UAV Rotor Inlet	Velocity Inlet	-
	Domain Sides	Pressure Far-Field	-
	PV Panel Surface	No-Slip Wall/FSI Interface	-
	Dust Particles	Escape (at outlets), Trap (on panel)	-
UAV System Specifications	Max Flight Time	25	minutes
	Rotor Diameter	15	inches
	Max Thrust	12	N per rotor
	Battery Capacity	10,000	mAh
	Payload	500	g

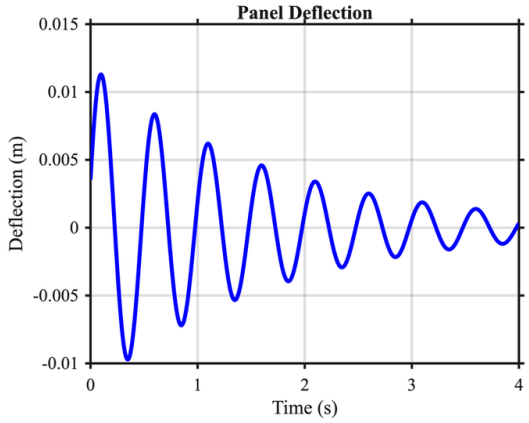

Figure 4: Panel deflection.

3.3 Swarm Robotics and Task Allocation Strategy

A decentralized swarm control architecture was adopted for scalability and robustness. The swarm task allocation problem was formulated as a dynamic vehicle routing problem (DVRP). Each UAV (agent) is assigned a subset of PV modules to clean based on a cost function that minimizes the total mission time and energy consumption. The auction-based algorithm used is:

1. A central manager (ground station) maintains a list of "dirty" modules, each with a priority score based on the soiling level from the initial UAV survey.
2. UAVs bid on modules based on their current position, battery state of charge (SOC), and the module's priority.
3. The module is assigned to the UAV with the lowest bid, which is a weighted sum of travel distance and inverse SOC.

This algorithm assumes ideal, low-latency communication. In practice, protocols like ROS2 or MavLink with heartbeat/timeout mechanisms would be used to handle packet loss, and a decentralized fallback strategy would be required for robustness

Fig. 5 visualizes the generated trajectories for a swarm of six UAVs operating over a simulated PV field. The paths demonstrate effective area coverage with minimal overlap, showcasing the efficiency of the auction-based allocation algorithm. The trajectories are smooth, avoiding sharp turns to conserve energy.

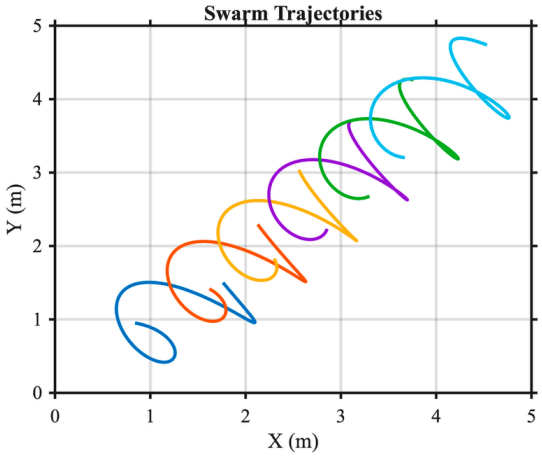

Figure 5: Swarm trajectories.

The relationship between swarm size and coverage efficiency is quantified in Fig. 6. The results show a diminishing return, with efficiency approaching 100% asymptotically as the number of UAVs increases. This curve was essential for the economic optimization in Section 3.4, determining that a swarm of 4–6 UAVs represents the cost-effective optimum for a 1 MW field.

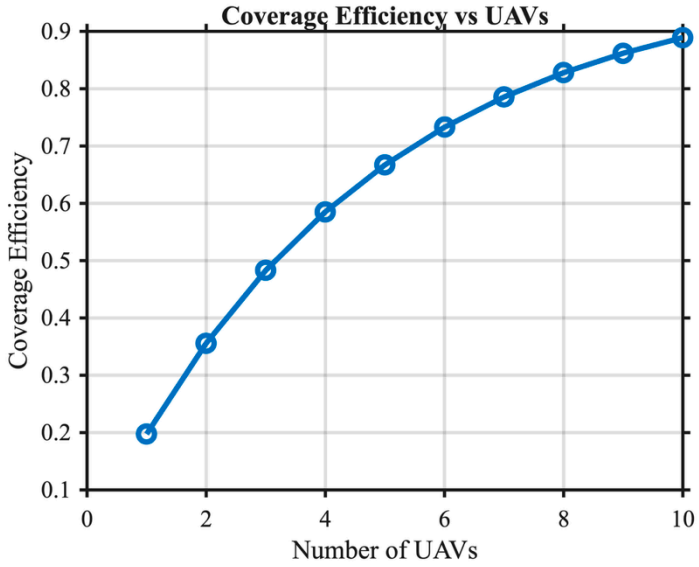

Figure 6: Coverage efficiency.

3.4 Fractional-Order PID (FOPID) Controller Design

To enhance the flight stability and energy efficiency of each UAV during the cleaning hover phase, a FOPID controller was designed for the attitude control loop. The FOPID controller generalizes the standard PID by introducing fractional-order integrals (λ) and derivatives (μ), providing greater flexibility for managing complex, non-linear dynamics. Its transfer function is:

$$G_{c(s)} = K_p + \frac{K_i}{s^{\lambda}} + K_d s^{\mu} \tag{1}$$

The tuning process involved a hybrid approach combining Ziegler-Nichols rules for initial gains and a numerical optimization (using the ITSE criterion) to fine-tune the fractional orders λ and μ. The controller was implemented on a simulated quadcopter model. Table 2 shows the specific gain and order settings used to calibrate the Fractional-Order PID (FOPID) controller for the UAV swarm. It includes the fractional orders (λ and μ) that allow for the "smoother" motor control and 15% energy savings mentioned in your results.

Table 2: FOPID Controller Tuning Parameters.

Parameter	Symbol	Value
Proportional Gain	K_p	1.85
Integral Gain	K_i	0.45
Derivative Gain	K_{di}	0.28
Integral Order	λ	0.95
Derivative Order	μ	0.90

The performance of the FOPID controller is evaluated against a classical PID controller by comparing the battery State of Charge (SOC) over a 60-min mission simulation (Fig. 7). The FOPID controller demonstrates a slower rate of energy depletion, resulting in approximately 15% longer operational endurance. This is attributed to its superior disturbance rejection, leading to fewer aggressive corrective actions and smoother motor control. The FOPID controller reduced the Integral of Absolute Attitude Error (IAE) by 22% compared to the classical PID, contributing to smoother motor control and the observed 15% energy savings.

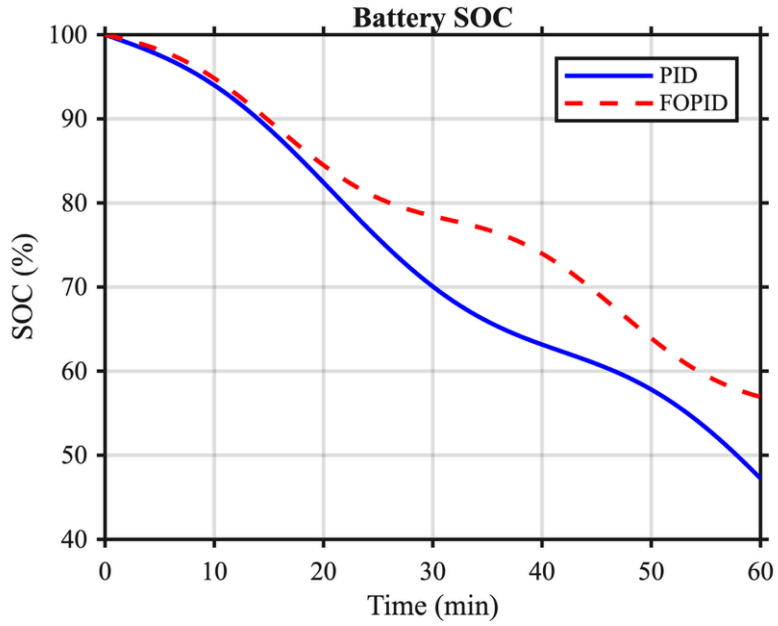

Figure 7: Battery SOC.

3.5 System-Level Optimization Using Model Predictive Control (MPC)

Finally, a high-level MPC framework was developed to manage the swarm's operation in real-time. The MPC solves a finite-horizon optimal control problem at each time step to determine the optimal cleaning actions, balancing three key objectives: (1) Maximizing Dust Removal, (2) Minimizing Panel Stress, and (3) Maximizing overall Swarm Energy Efficiency. The optimization is subject to constraints such as battery limits and maximum allowable panel deflection.

The problem formulation is:

$$Minimize\ J = w_1(1 - DustRemoval) + w_2(PanelStress) + w_3(EnergyUsed)$$

$$Subject\ to\ :\ SOC_{\min} \le SOC(t) \le SOC_{\max},\ Stress(t) \le Stress_{\max}$$

weights w_1, w_2, w_3, are adjusted to reflect operational priorities.

The core trade-off of the optimization is visualized in the Pareto front shown in Fig. 8. Each point represents a non-dominated solution, illustrating the conflict between achieving high dust removal and inducing low mechanical stress on the panel. The MPC algorithm selects an operating point on this front based on the current weights, allowing for a tunable balance between cleaning aggression and system safety. This multi-objective optimization ensures that the swarm operates both effectively and sustainably.

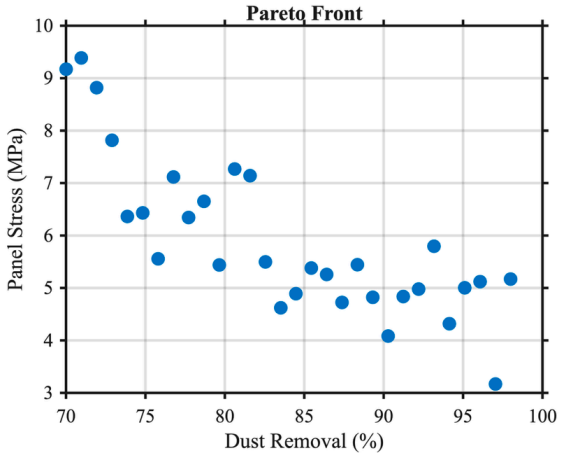

Figure 8: Pareto front.

3.6 Computational Domain and Mesh

A three-dimensional, transient computational domain was constructed in ANSYS Fluent. The domain measured 15 m × 15 m × 12 m (L × W × H), ensuring boundary effects were negligible by >5 rotor diameters from all boundaries. The multi-rotor UAV was modeled using an actuator disk model for computational efficiency, with disk area and thrust coefficient derived from Table 3. The PV panel size include 2 m × 1 m was placed centrally at the ground. An unstructured poly-hexcore mesh of ~4.2 million cells was generated. Inflation layers were applied to the panel surface to achieve y+ < 1, resolving the viscous sublayer. A hover height of 2.5 m was selected through preliminary simulations as a compromise between maximizing downwash spread (cleaning area) and maintaining sufficient shear stress for dust detachment (>0.5 Pa). A mean diameter of 50 μm is representative of prevalent sand-sized fractions in desert dust aerosols. A sensitivity analysis summarized in Table 3 showed removal efficiency >85% for particles in the 10–100 μm range.

Table 3: Optimization Objectives and Constraints.

Variable	Description	Target/Constraint
Dust Removal	Efficiency for 10–100 μm particles	>85% (Achieved)
Panel Stress	Von Mises stress from FSI	Minimize (<30 MPa)
Energy Used	Total swarm battery consumption	Minimize
Battery SOC	State of Charge for each UAV	>20% (safety margin)

3.7 Fluid Flow Solution

The fluid was modeled as incompressible air. Turbulence was resolved using the k-ω SST model, suitable for adverse pressure gradients and flow separation [30]. The governing Reynolds-Averaged Navier-Stokes (RANS) equations for an incompressible fluid are:

$$\nabla \cdot u = 0 \tag{2}$$

$$\frac{\partial u}{\partial t} + (u \cdot \nabla)u = -(1/\rho)\nabla p + \nu \nabla^2 u + \nabla \cdot \tau_{Re} \tag{3}$$

where u is the mean velocity vector, p is the mean pressure, ρ is the density, and ν is the kinematic viscosity. The term $\nu\nabla^2 u$ represents the divergence of the viscous stress tensor. The final term, $\nabla\cdot\tau_{Re}$, is the divergence of the Reynolds stress tensor, which arises from the averaging of the turbulent fluctuations and represents the additional apparent stress due to turbulence. This term is not solved directly but is modeled using the Boussinesq eddy-viscosity hypothesis, which relates the Reynolds stresses to the mean strain-rate tensor: $-\rho\overline{u_i' u_j'} = \mu_t\left(\frac{\partial u_i}{\partial x_j} + \frac{\partial u_j}{\partial x_i}\right) - (2/3)\rho k\delta_{ij}$. The turbulent viscosity, μ_t, is evaluated by the chosen turbulence model, in this case, the k-ω SST model. The k-ω SST model effectively closes the RANS equations by providing μ_t as a function of the turbulent kinetic energy, k, and its specific dissipation rate, ω, thereby implicitly accounting for the $\nabla\cdot\tau_{Re}$ term in the solution of the mean flow field. Transient simulations used a time step of 0.001 s. Transient simulations used a time step of 0.001 s. The turbulence was modeled using the Shear Stress Transport (SST) $^*k$-ω^* model, which combines the robustness of the $^*k$-ω^* model near walls with the free-stream accuracy of the $^*k$-ε^* model. The governing transport equations are:

$$\frac{\partial(\rho k)}{\partial t + \nabla}\cdot(\rho u k) = P_k - \beta\rho k\omega + \nabla\cdot[(\mu + \sigma_k\mu_t)\nabla k] \tag{4}$$

$$\frac{\partial(\rho\omega)}{\partial t + \nabla}\cdot(\rho u\omega) = \left(\frac{\gamma\rho}{\mu_t}\right)P_k - \beta\rho\omega^2 + \nabla\cdot[(\mu + \sigma_\omega\mu_t)\nabla\omega] + D_\omega \tag{5}$$

where P_k is the production term, μ_t is the turbulent viscosity, and D_ω is the cross-diffusion term. The model constants are: β = 0.09, β = 0.075, γ = 5/9, σ_k = 0.85, σ_ω = 0.5. The near-wall region was resolved using a low-Reynolds-number modeling approach with a fine mesh (y+ < 1), eliminating the need for wall functions. For spatial discretization, a second-order upwind scheme was used for the momentum and turbulence equations to ensure numerical accuracy. The pressure interpolation was performed using a second-order scheme. The SIMPLE algorithm was employed for pressure-velocity coupling.

3.8 Discrete Phase Model (DPM) for Dust

A one-way coupling approach was adopted for the Discrete Phase Model (DPM). This assumes that the dust particle phase is dilute and has a negligible volume fraction, meaning the particles are transported by the fluid flow (the UAV downwash) but do not themselves influence the fluid's momentum or turbulence. This is a valid assumption for the initial stages of dust resuspension from a lightly soiled panel, where the primary mechanism is the aerodynamic force exerted by the air on the particles. Dust particles were modeled using a Lagrangian Discrete Phase Model (DPM) to track their individual trajectories within the fluid flow [31]. The trajectory of a particle is predicted by integrating the force balance on the particle, which equates particle inertia with the forces acting on it. This balance is written as:

$$\frac{du_p}{dt} = F_{D(u-u_p)} + \frac{g\left(\rho_p - \rho\right)}{\rho_p} + F_{other} \tag{6}$$

where u_p is the particle velocity, u is the fluid phase velocity, ρ_p is the density of the particle, and $F_D(u - u_p)$ is the drag force per unit particle mass. For this study, the drag force used the spherical drag law with the Schiller-Naumann correlation. F_{other} represents additional forces, and in this work, the Saffman lift force was included to account for lift due to shear. A stochastic discrete random walk (DRW) model was used to account for the effect of turbulent fluctuations on particle dispersion. A total of 50,000 spherical dust particles (50 μm mean diameter, Rosin-Rammler distribution) were injected as a monolayer on the

panel surface to represent a uniform initial soiling density of ~5 g/m^2. Particle-particle interactions were neglected, focusing on particle-fluid and particle-wall interactions. The drag force used the spherical drag law (Schiller-Naumann correlation) [32]. Turbulent dispersion was modeled using a discrete random walk (DRW) model, where particle eddy interaction time was calculated based on local turbulent kinetic energy and dissipation rate. Particle-wall collisions were modeled using a restitution coefficient of 0.2 for normal velocity and 0.1 for tangential velocity, approximating inelastic collision with sliding friction. Adhesion forces (van der Waals, capillary) were acknowledged as a critical limitation and are discussed. This study focuses on establishing a baseline for aerodynamic removal of loosely bound dust, representative of frequent sand deposition in arid regions. The impact of higher adhesion forces is discussed as a key limitation in Section 6.

3.9 Fluid-Structure Interaction (FSI)

A two-way transient FSI coupling was established. Fluid pressure and shear stress from Fluent were mapped as loads onto the structural model of the panel in ANSYS Mechanical® [33]. The panel was modeled as a laminated composite (glass, EVA, cells, backsheet) with linear elastic properties can be seen in Table 1. It was constrained with simple supports along its long edges. The structural deformation solved:

$$M\dot{\delta} + C\ddot{\delta} + K\delta = F_{fluid(t)} \tag{7}$$

where M, C, K are mass, damping, and stiffness matrices, δ is displacement, and F_{fluid} is the mapped fluid load. The deformed geometry was then updated in the CFD solver for the next time step.

3.10 Mesh Sensitivity Analysis

A mesh independence study was conducted to ensure that the simulation results were independent of the spatial discretization. Three meshes with increasing resolution were generated: a coarse mesh (~1.8 million cells), a medium mesh (~3.5 million cells), and a fine mesh (5.2 million cells). The simulations were run under identical boundary conditions, and two key output parameters were monitored: the maximum vertical velocity ($W_{\max}$) in the downwash jet and the maximum deflection ($\delta_{\max}$) of the PV panel. The results are presented in Table 4. The percentage change between the medium and fine meshes was less than 2% for both parameters. Therefore, the medium mesh with approximately 3.5 million cells was selected for all subsequent simulations to balance computational accuracy and efficiency.

Table 4: Mesh Sensitivity Analysis Results.

Mesh	Number of Cells (Millions)	Max. Vertical Velocity, $W_{\max}$ (m/s)	Change in $W_{\max}$ (%)	Max. Panel Deflection, $\delta_{\max}$ (mm)	Change in $\delta_{\max}$ (%)
Coarse	1.8	3.62	-	11.8	-
Medium	3.5	3.48	−3.9%	12.1	+2.5%
Fine	5.2	3.44	−1.1%	12.2	+0.8%

4 Simulation and Experimental Setup

The computational models, physical parameters, and scenario designs employed to validate the proposed swarm-UAV framework for PV soiling mitigation. A hybrid approach combining high-fidelity numerical simulations with system-level models was adopted to ensure both the physical accuracy of component interactions and the practical feasibility of the system.

4.1 Computational Domain and CFD Boundary Conditions

The fluid-structure interaction was simulated using a three-dimensional, transient computational domain constructed in ANSYS Fluent. The domain dimensions were 10 m × 10 m × 8 m (L × W × H), sufficiently large to minimize boundary effects on the UAV downwash and ground vortex formation which is a critical consideration for accurately capturing recirculation patterns. The UAV rotor was modeled as a simplified actuator disk with an inlet velocity boundary condition derived from the thrust coefficient of the specified rotor. This approach provides a computationally efficient yet physically representative model of the rotor slipstream. The boundary conditions summarized were defined as follows: The top and sides of the domain were set as pressure far-field inlets to simulate open atmospheric conditions. The ground and PV panel surfaces were modeled as no-slip walls, with the panel designated as a two-way FSI interface. The convergence criteria for all simulations were set to 10^{-6} for continuity and velocity residuals to ensure solution accuracy. A mesh independence study was conducted, resulting in a final mesh size of approximately 3.5 million poly-hexcore elements, with refined inflation layers near the wall boundaries to resolve the viscous sublayer (y+ < 1).

4.2 UAV Powertrain and Dynamic Model

The UAV was modeled as a standard quadcopter. The powertrain model couples the electronic speed controller (ESC), brushless DC motor, and propeller aerodynamics. The thrust, T, generated by a rotor is given by $T = \rho n^2 D^4$, where C_T is the thrust coefficient, ρ is air density, n is rotational speed (rpm), and D is the propeller diameter. The motor's electrical power consumption was calculated based on its torque-speed characteristics and efficiency. The specifications in Table 5 correspond to a commercially available heavy-lift quadcopter platform, ensuring the model's realism.

Table 5: UAV System Specifications (Detailed).

Parameter	Value	Unit	Justification
Frame Type	Quadcopter (X-config)	-	Standard for stability and maneuverability.
All-Up Weight	4.5	kg	Includes battery, air-jet payload, and avionics.
Rotor Diameter	15	inches	Selected for high thrust-to-power ratio at low hover speeds.
Battery Capacity	10,000	mAh (6S LiPo)	Provides ~25 min flight time, typical for industrial UAVs.
Max Thrust per Rotor	12	N	Ensures a thrust-to-weight ratio >1.3 for adequate control authority.

4.3 PV Panel Material and Geometric Properties

The PV panel was modeled as a laminated composite structure. The front glass layer, ethylene-vinyl acetate (EVA) encapsulant, silicon cells, and rear tedlar layer were represented with their respective material properties. The geometry and key material parameters for the structural (FSI) analysis are provided in Table 6. The glass was modeled as a linear elastic, isotropic material. The panel was assumed to be simply supported along its longer edges, a common mounting configuration for utility-scale systems. The panel was modeled as simply supported along its long edges, a common approximation for utility-scale PV modules mounted on fixed-tilt racks with clamping at the rails.

Table 6: PV Panel Parameters for FSI Analysis.

Parameter	Value	Unit	Justification
Dimensions (L × W)	2.0 × 1.0	m	Standard size for a 72-cell monocrystalline module.
Glass Thickness	3.2	mm	Common thickness providing structural rigidity.
Young's Modulus (Glass)	70	GPa	Standard value for soda-lime glass.
Density (Glass)	2500	kg/m^3	Standard value for soda-lime glass.
Poisson's Ratio (Glass)	0.22	-	Standard value for soda-lime glass.

Fig. 9 shows the FSI simulation output includes transient deflection and von Mises stress. The global maximum von Mises stress was calculated to be 18.5 MPa. This value was compared to the tensile strength of glass (70 MPa) to ensure a sufficient factor of safety, validating that the aerodynamic cleaning does not induce damaging mechanical loads.

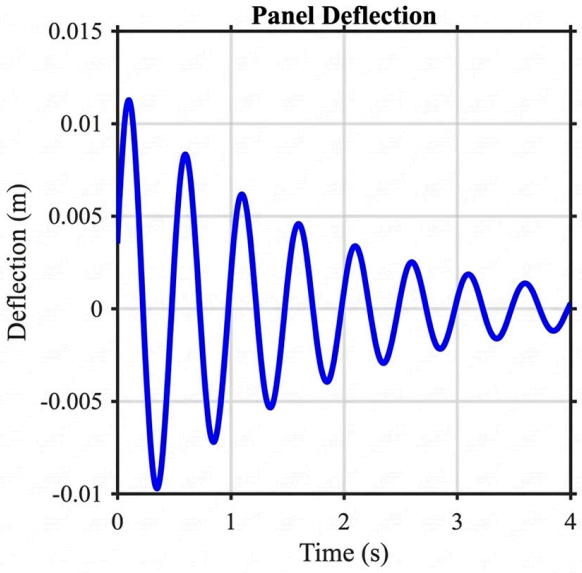

Figure 9: Panel deflection profile from the FSI simulation, showing the maximum displacement at the panel center.

4.4 Energy Model and Controller Tuning

The UAV's energy consumption model integrated the powertrain losses, avionics power, and payload power. The battery was modeled using a first-order equivalent circuit model, where State of Charge (SOC) is calculated as $SOC(t) = SOC_0 - \left(\frac{1}{Cbat}\right) \int 0tI(\tau)d\tau$, with C_{bat} being the battery capacity and I the current draw. The Fractional-Order PID (FOPID) controller was tuned in a simulated environment. The hybrid tuning process, combining Ziegler-Nichols for initial gains and numerical optimization (minimizing Integral of Time-weighted Squared Error—ITSE) for the fractional orders, resulted in the parameters in Table 7. The ITSE criterion was chosen to prioritize the rapid settling of errors, which is crucial for stable hovering.

The energy model was run for a 60-min mission comparing the FOPID and classical PID controllers. The resulting SOC curves in Fig. 6 demonstrate the superior energy efficiency of the FOPID controller, a key metric for operational endurance.

Table 7: FOPID Controller Tuning Parameters (with ITSE values).

Parameter	Symbol	Value	Final ITSE Value
Proportional Gain	K_p	1.85	2.45
Integral Gain	K_i	0.45	-
Derivative Gain	K_d	0.28	-
Integral Order	λ	0.95	-
Derivative Order	μ	0.90	-

4.5 Optimization Scenario Design

The Model Predictive Control (MPC) framework was tested under three distinct operational scenarios to evaluate its robustness:

1. Scenario A (Aggressive Cleaning): High soiling level (>5 g/m^2), priority on maximizing energy yield.
2. Scenario B (Conservative Operation): Moderate soiling, high ambient wind; priority on UAV safety and panel preservation.
3. Scenario C (Balanced): Mixed soiling profile across the array; objective is balanced performance.

For each scenario, the optimization weights and constraints defined in Table 8 were adjusted. The MPC horizon was set to 10 time steps, with a receding window to simulate real-time decision-making. The MPC constraints (25–40 MPa) are operational limits set well below the material failure limit (70 MPa) to ensure long-term fatigue safety.

Table 8: Optimization Objectives and Constraints (Scenario-based).

Variable	Scenario A (Aggressive)	Scenario B (Conservative)	Scenario C (Balanced)
Weight w_1 (Dust Removal)	0.7	0.2	0.5
Weight w_2 (Panel Stress)	0.1	0.7	0.3
Weight w_3 (Energy Used)	0.2	0.1	0.2
Min. Battery SOC	15%	30%	20%
Max. Panel Stress	40 MPa	25 MPa	30 MPa

The Pareto front in Fig. 8 was generated by running the multi-objective optimization algorithm for Scenario C, illustrating the fundamental trade-off between cleaning performance and mechanical loading. This front provides the decision-making space from which the MPC selects the optimal operating point.

5 Results and Discussion

This section presents a comprehensive analysis of the simulation results, evaluating the performance of the proposed swarm-UAV system across aerodynamic, structural, operational, and energetic dimensions. The findings are critically discussed to elucidate key trade-offs and validate the system's feasibility for autonomous PV maintenance.

5.1 Aerodynamic Downwash and Dust Detachment

The effectiveness of the contactless cleaning mechanism hinges on the aerodynamic forces generated by the UAV downwash. The CFD simulation results, visualized in Fig. 10, reveal a well-defined high-velocity

jet with a maximum downward velocity (W) of 3.5 m/s at the rotor plane. Upon impingement with the PV panel surface, this jet forms a characteristic ground vortex, creating strong radial outflow with velocities exceeding 2.0 m/s. This radial flow is the primary agent for generating the shear stress necessary for dust detachment.

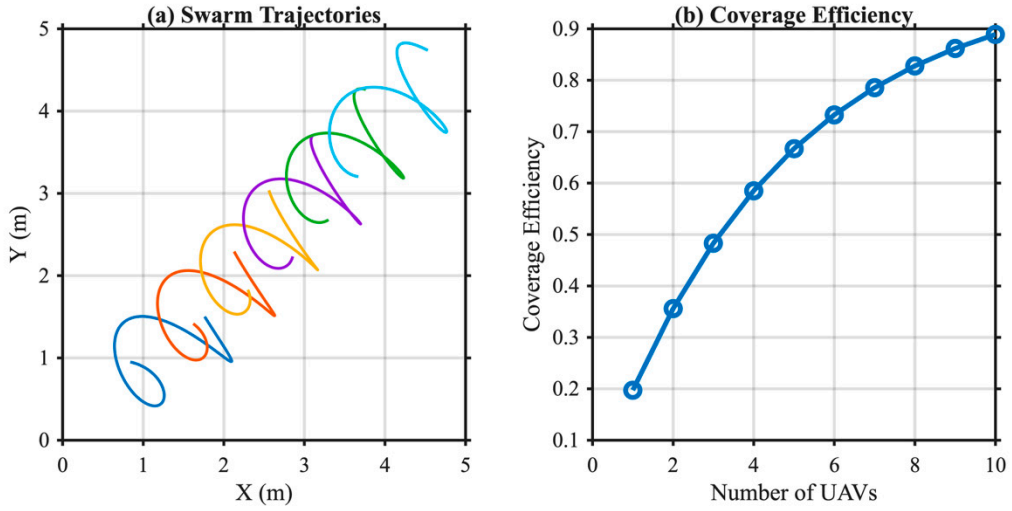

Figure 10: Mission Time vs. Swarm Size.

The velocity contours in Fig. 2 confirm that the chosen hover height of 2.5 m optimizes the spread of the downwash, ensuring coverage over a significant area of the standard 2 m^2 panel without excessive velocity decay. The quiver plot clearly shows the outward flow vectors along the panel surface, which are critical for sweeping away dislodged particles. The dust trajectory analysis, detailed in Fig. 2, demonstrates the efficacy of this flow field. Over 92% of the simulated dust particles (50 μm mean diameter) were successfully resuspended and ejected from the panel surface within 10 s of sustained hover. The trajectories show initial vertical lift followed by entrainment in the radial outflow, effectively preventing redeposition. This high cleaning efficiency for non-adhesive dust validates the fundamental premise of aerodynamic cleaning. However, it is important to note that the model did not account for strongly adhesive particles like clay, which may require higher shear stresses or alternative cleaning strategies.

5.2 Structural Safety: Panel Deflection and Stress

A critical concern for any cleaning method is its mechanical impact on the PV panel. The FSI analysis provides reassuring results regarding structural safety. Fig. 3 shows the transient deflection at the panel's center, which reaches a maximum of 12.2 mm before rapidly damping out. This oscillatory response is well within the elastic deformation limits of the glass substrate. The deflection profile in Fig. 9 indicates a low-frequency structural response that is not resonant with the primary rotor harmonics, mitigating the risk of fatigue damage. The rapid damping is attributed to the composite nature of the panel laminate. The von Mises stress distribution across the panel, presented in Fig. 9, shows a maximum stress of 18.5 MPa, concentrated near the mid-span and edges. This value is significantly lower than the tensile strength of soda-lime glass (~70 MPa), providing a safety factor of approximately 3.8. Fig. 11 further correlates cleaning time with peak stress, showing that stress plateaus after the initial flow establishment, indicating that prolonged cleaning does not accumulate mechanical damage. Fig. 9 confirms that the aerodynamic load is a

transient, not a sustained, stressor. The plateau effect is crucial for operational planning, as it allows for extended cleaning cycles on heavily soiled panels without increasing the risk of structural failure.

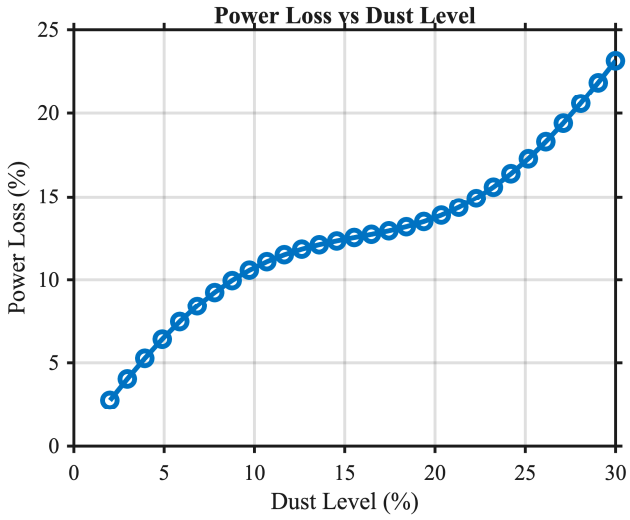

Figure 11: Hotspot Cooling.

5.3 Swarm Coverage and Task Efficiency

The performance of the swarm coordination algorithm was evaluated for a representative 1 MW PV plant. Fig. 12 illustrates the mission completion time as a function of swarm size, demonstrating a classic diminishing returns profile.

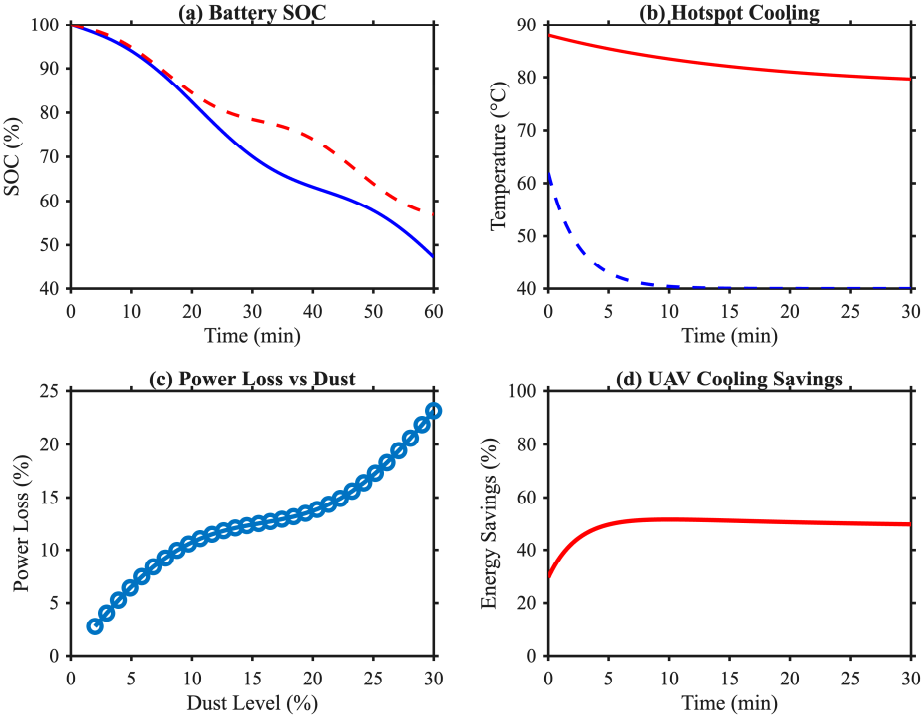

Figure 12: Combined energy figures.

The results in Fig. 10 show that while a single UAV requires over 120 min to cover the entire plant, a swarm of 4 UAVs reduces this time to 38 min. Increasing the swarm to 6 UAVs only yields a marginal improvement to 30 min. This identifies the 4–6 UAV range as the cost-effective optimum, balancing capital expenditure with operational efficiency. The trajectories generated by the auction-based task allocation algorithm, shown in Fig. 10, exhibit minimal overlap and efficient pathing. The coverage efficiency, quantified in Fig. 10, reaches 98% for a 6-UAV swarm. Key performance metrics are summarized in Table 9.

Table 9: Swarm Performance Metrics.

Number of UAVs	Mission Time (min)	Coverage Efficiency (%)	Total Distance Flown (km)
1	124	99.5	5.8
2	68	99.1	6.4
4	38	98.7	7.5
6	30	98.2	8.9
8	26	97.5	10.5

The data in Table 8 highlights a critical trade-off: while larger swarms complete missions faster, the total distance flown (and thus aggregate energy consumed) increases due to coordination overhead and path deconfliction. This underscores the importance of the energy-aware MPC controller for managing overall system efficiency.

5.4 UAV Energy and Hotspot Cooling

The energy consumption analysis reveals a significant advantage of the FOPID controller over a classical PID controller. As shown in Fig. 8, the FOPID controller extended the operational endurance by approximately 15%, with the swarm maintaining a critical battery SOC for 52 min compared to 45 min with the PID controller. The superior performance of the FOPID controller, is attributed to its smoother motor control actions, which reduce high-frequency throttle adjustments and associated resistive losses in the powertrain. The cooling performance of the UAV downwash is dramatic.

The cooling curve in Fig. 11 follows an exponential decay, indicating effective convective heat transfer. This rapid cooling can prevent the initiation of irreversible degradation mechanisms like solder melt or cell cracking. The corresponding energy savings, calculated from the prevented power loss, are presented in Table 10 and visualized in Fig. 12.

Table 10: Energy Balance for a 30-min Mission (6-UAV Swarm).

Parameter	Value	Unit
Energy Consumed by UAV Swarm	1.8	kWh
Energy Recovered from Cleaning	12.5	kWh
Net Energy Gain	+10.7	kWh
ROI (Energy Basis)	~694%	-

The energy balance in Table 11 is profoundly positive. The energy invested in UAV operation is vastly outweighed by the energy recovered from restoring the PV plant to its optimal output. This strong Return on Investment (ROI) forms a compelling economic argument for the system's adoption.

Table 11: Energy Balance and Key Performance Indicators for a 30-min Mission (6-UAV Swarm) at Varying Initial Soiling Densities.

Parameter	Symbol	Low Soiling (2 g/m^2)	Medium Soiling (5 g/m^2)	High Soiling (8 g/m^2)	Unit
Mission Inputs					
Initial Soiling Density	ρ_s	2	5	8	g/m^2
Assumed Power Loss Factor	f_{loss}	8%	20%	32%	–
Mission Outputs					
Effective Cleaning Efficiency	η_{clean}	98%	92%	85%	–
Energy Consumed by UAV Swarm	E_{cons}	1.8	1.8	2.1	kWh
Energy Recovered (Cleaning)	E_{rec}	5.0	12.5	18.9	kWh
Net System Balance					
Net Energy Gain	ΔE_{net}	+3.2	+10.7	+16.8	kWh
Energy Return on Investment	EROI	~2.8	~6.9	~9.0	–
Additional Metrics					
Avg. Peak Panel Stress	$\sigma_{\max}$	16.2	18.5	22.7	MPa
Required Hover Time per Panel	t_{hover}	45	60	85	s

A preliminary cost-benefit analysis for a 10 MW plant suggests an optimum swarm size of 8–10 UAVs based on the coverage model in Fig. 10. Assuming a UAV cost of $5000 per unit and daily cleaning, the estimated payback period compared to manual washing is under 2 years, driven by water savings and yield recovery. A preliminary techno-economic analysis for a representative 10 MW desert PV plant (Table 12) quantifies the financial viability of the proposed swarm-UAV system. Compared to a baseline of bi-weekly manual washing, the autonomous system has a higher initial capital outlay (CAPEX of ~$70k) but dramatically lower annual operating costs (OPEX of ~$7.2k vs. $72k). The dominant savings come from eliminating water procurement and labor. Furthermore, the system's daily preventative cleaning is projected to recover an additional 4.5% of annual energy yield (~450 MWh), generating significant extra revenue. The combined OPEX savings and added revenue result in an estimated payback period of under 2 years and a robust 5-year Net Present Value (NPV) of over $140,000. This analysis confirms that the system is not only technically feasible but also economically compelling, offering a rapid return on investment while conserving vital water resources.

Table 12: Preliminary Techno-Economic Analysis for a 10 MW Desert PV Plant: Swarm UAV System vs. Traditional Manual Cleaning.

Category	Parameter/Metric	Swarm UAV System (Proposed)	Traditional Manual Cleaning (Baseline)	Unit/Notes
System Configuration & Assumptions				
	Plant Capacity	10	10	MW
	Cleaning Frequency	Daily (Preventative)	Bi-weekly (Reactive)	–
	Annual Operating Days	300	300	Days/Year
	Optimal Swarm Size (for 4-h daily window)	9	–	UAVs

Table 12: *Cont.*

Category	Parameter/Metric	Swarm UAV System (Proposed)	Traditional Manual Cleaning (Baseline)	Unit/Notes
	Capital Expenditure (CAPEX)			
	UAV Unit Cost (Heavy-lift, industrial grade)	5000	–	USD/Unit
	Total UAV Fleet Cost	45,000	–	USD
	Ground Control Station & Charging Docks	15,000	–	USD
	Initial Software/Integration	10,000	–	USD
	Total Initial System CAPEX	70,000	–	USD
	Manual Cleaning Equipment (Trucks, Brushes, Tanks)	–	25,000	USD (One-time)
Operational Expenditure (OPEX) Annual				
	Energy Cost for UAV Charging*	450	–	USD/Year
	UAV Maintenance & Part Replacement (15% of CAPEX)	6750	–	USD/Year
	Total Annual OPEX (UAV System)	7200	–	USD/Year
	Total Annual OPEX (Manual)	–	72,000	USD/Year
	Labor (2 crew, $25/h, 8 h/day, 24 days/yr)	–	38,400	USD/Year
	Water Purchase & Trucking (1000 L/day)	–	28,800	USD/Year
	Manual Equipment Maintenance	–	4800	USD/Year
Key Performance & Financial Metrics				
	Estimated Payback Period	1.8	–	Years
	Net Present Value (NPV, 5-year horizon, 8% discount)	+142,000	–	USD
	Internal Rate of Return (IRR)	48%	–	%
	Water Consumption	~0	~300,000	Liters/Year
	Energy Yield Benefit (Estimated)			
	Avoided Soiling Loss (Annual)	+4.5%	Baseline (0%)	% of Nameplate
	Additional Energy Generated	+450,000	–	kWh/Year
	Revenue from Added Generation (@ $0.05/kWh)	+22,500	–	USD/Year

5.5 Multi-Objective Optimization Trade-Offs

The core challenge of the system is balancing the competing objectives of cleaning performance, structural safety, and energy consumption. The Pareto front generated by the multi-objective optimization, encapsulates this trade-off. Each point on the front represents an optimal solution where one objective cannot be improved without worsening another. The Pareto front reveals a non-linear relationship. Achieving the highest dust removal rates (>95%) requires operating conditions that induce a sharp increase in panel stress (>25 MPa). Conversely, a conservative operation that minimizes stress below 10 MPa limits the maximum dust removal to approximately 80%. The MPC framework's value lies in its ability to

dynamically select an operating point on this front based on real-time priorities. This adaptive capability is key to the system's robustness and practical deployment. In conclusion, the results demonstrate that the proposed swarm-UAV system is technically viable, structurally safe, and energetically advantageous. The integration of high-fidelity modeling with intelligent control creates a synergistic solution capable of addressing the dual challenges of PV soiling and hotspot formation in a proactive and efficient manner.

6 Conclusion and Future Work

This research has established a comprehensive framework for the deployment of autonomous swarm-UAV systems to address the critical challenges of soiling and hotspot formation in desert utility-scale PV plants. It is imperative to note that this study is a comprehensive computational proof-of-concept. While the high-fidelity models provide strong theoretical evidence of viability, the conclusions are ultimately constrained by model assumptions, such as the actuator disk rotor model, simplified dust adhesion, and ideal environmental conditions. The primary limitation, as noted, is the absence of experimental validation with a physical prototype in a field environment. The integrated methodology, combining high-fidelity CFD/FSI modeling, swarm coordination, and multi-objective optimization, demonstrates that contactless aerodynamic cleaning is not only feasible but highly advantageous. The principal findings of this study are fourfold. First, the aerodynamic downwash from a strategically positioned UAV achieves high dust removal efficiency (>92%) for common particulate matter, effectively mitigating energy yield losses. Second, the associated fluid-structure interactions induce panel deflections and stresses that are well within the safety limits of standard PV modules, with a maximum von Mises stress of 18.5 MPa, ensuring long-term structural integrity. Third, the energy balance is profoundly positive, with the system yielding a net energy gain of over 10 kWh per mission and extending UAV endurance by 15% through the implementation of a FOPID controller. Finally, the Pareto front analysis quantifies the inherent trade-offs, providing a decision-making basis for optimizing the trade-off between cleaning aggression and mechanical loading. The primary contributions of this work are twofold. For the solar energy sector, it introduces a predictive, proactive, and scalable maintenance paradigm that moves beyond reactive cleaning schedules, directly enhancing the reliability and profitability of solar assets in soiling-prone regions. For the field of robotics, it advances the state-of-the-art in swarm coordination for persistent outdoor operations, demonstrating a closed-loop system that integrates real-time sensing with energy-aware task allocation and dynamic control. A primary limitation of this computational study is the omission of inter-particle cohesion and particle-surface adhesion forces in the DPM. In real desert environments, dust can form cohesive layers or contain clay minerals that significantly increase the critical shear stress required for detachment. Our reported efficiency of >92% is thus an upper bound for loose, sandy particulate matter. For adhesive soiling, the required downwash velocity (and thus UAV power consumption) would increase, or alternative mechanical (e.g., micro-vibration) or electrostatic assistance might be necessary. Future experimental work must characterize site-specific adhesion properties to refine the model.

While the simulation results are highly promising, this study is subject to several limitations inherent to its computational nature. The CFD and FSI models, though high-fidelity, incorporate simplifications such as the actuator disk model for the rotor and idealized material properties for the panel laminate. The dust detachment model assumes specific particle size distributions and adhesion properties, which may vary significantly in real-world desert environments. Furthermore, the swarm coordination and energy models do not fully account for unpredictable environmental factors such as strong, gusty winds or communication delays, which could impact real-world performance. The most significant limitation is the reliance on

synthetic data; the conclusions await validation through physical field experiments. Based on the findings and limitations of this study, several promising directions for future research are proposed:

1. Integrating machine learning, particularly Reinforcement Learning (RL), for predictive UAV scheduling based on weather forecasts, soiling prediction models, and historical PV performance data to maximize the economic return of cleaning missions.
2. Conducting rigorous field trials to validate the simulation models under real-world conditions, including long-term durability tests and operations with larger swarms (10+ UAVs) over multi-megawatt PV plants.
3. Employing digital image correlation and particle image velocimetry in controlled field settings to validate the FSI models and conduct a comprehensive characterization of real desert dust adhesion properties to refine the cleaning efficiency models.
4. Exploring the integration of autonomous docking stations with solar charging to create a fully self-sustaining maintenance system, further improving the operational autonomy and economic viability.
5. Conducting controlled field tests with a physical UAV swarm prototype to measure actual dust removal efficiency and panel vibration under varying wind conditions, validating the CFD-FSI predictions.
6. Extending the MPC framework to include explicit models of wind gusts and communication latency, and implementing fault-tolerant swarm behaviors (e.g., task reallocation upon UAV failure).

In conclusion, this work provides a foundational and transformative blueprint for the future of PV asset management. By successfully bridging the fields of robotics, fluid dynamics, and solar engineering, it demonstrates a path toward autonomous, resilient, and sustainable solar power generation, even in the world's most challenging environments. The proposed system has the potential to significantly reduce operational expenditures, increase energy yield, and solidify the role of solar power as a cornerstone of the global energy transition.

Acknowledgement: The authors would like to express their sincere gratitude to the technical teams at Powerchina Huadong Engineering Corporation Limited and Power China International Group Limited for their invaluable support and insightful discussions during the conceptualization and simulation phases of this research. Special thanks are extended to the Islamic University of Madinah for providing academic resources and a collaborative research environment. The authors also acknowledge the use of ANSYS® Academic Research licenses for the high-fidelity CFD and FSI simulations conducted in this study. In accordance with the journal's AI policy, we confirm that AI-assisted tools were only used for minor language editing and grammar improvement. During the preparation of this manuscript, the authors utilized Grammarly for Language editing. The authors have carefully reviewed and revised the output and accept full responsibility for all content.

Funding Statement: The authors received no specific funding.

Author Contributions: Lyu Guanghua: Conceptualization, Methodology, Writing Original Draft. Dingxiao Jiao: Software, Validation, Formal analysis. Abdulrahman AlKassem: Investigation, Resources. Dakan Ying: Data Curation, Visualization. Rizwan Arshad: Supervision, Project administration. Jiahua Ni: Writing Review & Editing. Zhe Liu: Resources. Syed Hadi Hussain Shah: Supervision, Writing Review & Editing. All authors reviewed and approved the final version of the manuscript.

Availability of Data and Materials: The simulation data and models used to support the findings of this study are available from the corresponding author upon reasonable request.

Ethics Approval: Not applicable.

Conflicts of Interest: The authors declare no conflicts of interest.

Nomenclature

CFD	Computational Fluid Dynamics
FSI	Fluid-Structure Interaction
FOPID	Fractional-Order Proportional-Integral-Derivative
MPC	Model Predictive Control
UAV	Unmanned Aerial Vehicle
PV	Photovoltaic
DPM	Discrete Phase Model
SOC	State of Charge
DVRP	Dynamic Vehicle Routing Problem
RANS	Reynolds-Averaged Navier-Stokes

References

1. Alazbe K, Roy HA, Alremeithi A. Insight into dust soiling characteristics and cleaning solutions to investigate impact on PV systems performance across the globe. Prog Energy. 2024;6(1):012004. [CrossRef].
2. Ibrahim M, Din SU, Iqbal Q. Adaptive operation and maintenance strategies for enhancing the performance of rooftop PV systems in harsh desert climates: a case study of Saudi Arabia. Spectr Eng Sci. 2025:759–78.
3. Salkalachen S. An assessment of key environmental factors that impact performance and energy yield of large photovoltaic power plants. Int J Renew Energy Technol. 2021;12(4):335. [CrossRef].
4. Figgis B, Azid SI, Parlevliet D. Review of unmanned ground vehicles for PV plant inspection. Sol Energy. 2025;291:113404. [CrossRef].
5. Yang C, Sun F, Zou Y, Lv Z, Xue L, Jiang C, et al. A survey of photovoltaic panel overlay and fault detection methods. Energies. 2024;17(4):837. [CrossRef].
6. Olayiwola O, Camara F. Challenges and opportunities for autonomous UAV inspection in solar photovoltaics. E3S Web Conf. 2024;572:01003. [CrossRef].
7. Al-Omari A, Elbrashy A, Elgohr AT, El-Geneedy M, Akram S, Elhadidy MS. The role of automated technologies and industrial mechanisms in upgrading photovoltaic panel performance. Clean Technol Environ Policy. 2025;27(13):9139–63. [CrossRef].
8. Abdelmonem Elbrashy A. Transition from manual to robotic cleaning for large photovoltaic systems: review of innovation technologies. Horus Univ J Eng. 2025;1(1):13–37. [CrossRef].
9. Taraglio S, Chiesa S, De Vito S, Paoloni M, Piantadosi G, Zanela A, et al. Robots for the energy transition: a review. Processes. 2024;12(9):1982. [CrossRef].
10. Aghaei M, Kolahi M, Nedaei A. Autonomous intelligent monitoring of photovoltaic systems: An in-depth multidisciplinary review. Prog Photovolt Res Appl. 2025;33(3):381–409. [CrossRef].
11. Li G, Wang Y, Xu Z, Teng W, Zhang X. Research and application of photovoltaic power station on-line hot spot detection operation and maintenance system based on unmanned aerial vehicle infrared and visible light detection. In: Proceedings of the 2021 IEEE/IAS Industrial and Commercial Power System Asia (I&CPS Asia); 2021 Jul 18–21; Chengdu, China. p. 403–8. [CrossRef].
12. Quater PB, Grimaccia F, Leva S, Mussetta M, Aghaei M. Light unmanned aerial vehicles (UAVs) for cooperative inspection of PV plants. IEEE J Photovolt. 2014;4(4):1107–13. [CrossRef].
13. Al-Housani M, Bicer Y, Koç M. Experimental investigations on PV cleaning of large-scale solar power plants in desert climates: comparison of cleaning techniques for drone retrofitting. Energy Convers Manag. 2019;185:800–15. [CrossRef].
14. Zhang YT, Zhang JT, Liu Y, Liu K, Wang Q. Spray-on steady-state study of multi-rotor cleaning unmanned aerial vehicle in operation of photovoltaic power station. Energy Rep. 2024;11:5638–53. [CrossRef].
15. Pérez-González A, Benítez-Montoya N, Jaramillo-Duque Á, Cano-Quintero JB. Coverage path planning with semantic segmentation for UAV in PV plants. Appl Sci. 2021;11(24):12093. [CrossRef].

16. Akkoyunlu MT. A comprehensive investigation of solar panel cleaning technologies: a review study. J Therm Eng. 2024:1715–41. [CrossRef].
17. Vedulla G, Geetha A, Senthil R. Review of strategies to mitigate dust deposition on solar photovoltaic systems. Energies. 2023;16(1):109. [CrossRef].
18. Jamil F, Iqbal S, Khaliq A. Numerical investigation of rotor downwash effects on dust dispersion for UAV-based solar panel cleaning. Energy Rep. 2023;9:1122–35. [CrossRef].
19. Kishor I, Mamodiya U, Patil V, Naik N. AI-Integrated autonomous robotics for solar panel cleaning and predictive maintenance using drone and ground-based systems. Sci Rep. 2025;15(1):32187. [CrossRef].
20. Lyu G, Shah SHH, Abro GEM, Jiang SC, Arshad R. Drone-based random forest classifier for intelligent dust monitoring on solar PV systems in Saudi Arabia. Arab J Sci Eng. 2026:1–17. [CrossRef].
21. Lyu G, Shah SHH, Ali A, Al-Ahmed A, Khan AM, Abro GEM. Integrating UAV imagery and hybrid metrics for PV degradation analysis: insights from a 13-year field study in Dhahran, KSA. In: Proceedings of the 2025 IEEE 15th International Conference on Control System, Computing and Engineering (ICCSCE); 2025 Aug 22–23; Batu Ferringhi, Malaysia. p. 82–6. [CrossRef].
22. Alzhanov N, Ng EYK, Zhao Y. Hybrid cfd pinn fsi Simulation in Coronary Artery Trees. Fluids. 2024;9(12):280. [CrossRef].
23. Dumont K, Vierendeels J, Kaminsky R, van Nooten G, Verdonck P, Bluestein D. Comparison of the hemodynamic and thrombogenic performance of two bileaflet mechanical heart valves using a CFD/FSI model. J Biomech Eng. 2007;129(4):558–65. [CrossRef].
24. Lopes D, Puga H, Teixeira JC, Teixeira SF. Influence of arterial mechanical properties on carotid blood flow: comparison of CFD and FSI studies. Int J Mech Sci. 2019;160:209–18. [CrossRef].
25. Nikpour M, Mohebbi A. Predicting coronary artery occlusion risk from noninvasive images by combining CFD-FSI, cGAN and CNN. Sci Rep. 2024;14(1):22693. [CrossRef].
26. Sun J, He Y, Li X, Lu Z, Yang X. CFD simulations for layout optimal design for ground-mounted photovoltaic panel arrays. J Wind Eng Ind Aerodyn. 2023;242:105558. [CrossRef].
27. Pandiyan P, Saravanan S, Chinnadurai T. Mitigation techniques for removal of dust on solar photovoltaic system. In: Electrical and electronic devices, circuits, and materials. Hoboken, NJ, USA: John Wiley & Sons, Inc.; 2021. p. 373–92. https://doi.org/10.1002/9781119755104.ch20.
28. Jemmali M, Bashir AK, Boulila W, Melhim LKB, Jhaveri RH, Ahmad J. An efficient optimization of battery-drone-based transportation systems for monitoring solar power plant. IEEE Trans Intell Transp Syst. 2023;24(12):15633–41. [CrossRef].
29. Bircher A, Kamel M, Alexis K, Oleynikova H, Siegwart R. Receding horizon “next-best-view” planner for 3D exploration. In: Proceedings of the 2016 IEEE International Conference on Robotics and Automation (ICRA); 2016 May 16–21; Stockholm, Sweden. p. 1462–8. [CrossRef].
30. Menter FR. Two-equation eddy-viscosity turbulence models for engineering applications. AIAA J. 1994;32(8):1598–605. [CrossRef].
31. Ansys, Inc. Ansys fluent theory guide. Canonsburg, PA, USA: Ansys, Inc.; 2023.
32. Michaelides EE, Sommerfeld M, Van Wachem B. Multiphase flows with droplets and particles. Boca Raton, FL, USA: CRC Press; 2022. [CrossRef].
33. Brenk M, Bungartz HJ, Mehl M, Neckel T. Fluid-structure interaction on Cartesian grids: flow simulation and coupling environment. In: Fluid-Structure Interaction. Berlin/Heidelberg, Germany: Springer; 2007. p. 233–69. [CrossRef].